

Dynamic Interference Management for TN–NTN Coexistence in the Upper Mid-Band

Pradyumna Kumar Bishoyi[†], Chia Chia Lee^{*}, Navid Keshtiarast^{*}, and Marina Petrova^{*}

[†]Department of Electrical Engineering, Indian Institute of Technology Jodhpur, Rajasthan, India

^{*}Chair of Mobile Communications and Computing (MCC), RWTH Aachen University, Aachen, Germany

Emails: pradyumna@iitj.ac.in, {chia.lee, navid.keshtiarast, petrova}@mcc.rwth-aachen.de

Abstract—The coexistence of terrestrial networks (TN) and non-terrestrial networks (NTN) in the frequency range 3 (FR3) upper mid-band presents considerable interference concerns, as dense TN deployments can severely degrade NTN downlink performance. Existing studies rely on interference-nulling beamforming, precoding, or exclusion zones that require accurate channel state information (CSI) and static coordination, making them unsuitable for dynamic NTN scenarios. To overcome these limitations, we develop an optimization framework that jointly controls TN downlink power, uplink power, and antenna downtilt to protect NTN links while preserving terrestrial performance. The resultant non-convex coupling between TN and NTN parameters is addressed by a Proximal Policy Optimization (PPO)-based reinforcement learning method that develops adaptive power and tilt control strategies. Simulation results demonstrate a reduction up to 8 dB in the median interference-to-noise ratio (INR) while maintaining over 87% TN basestation activity, outperforming conventional baseline methods and validating the feasibility of the proposed strategy for FR3 coexistence.

Index Terms—Terrestrial Network, Non-terrestrial Networks, Upper mid band, Frequency Range 3, Interference management

I. INTRODUCTION

The rapid growth in global mobile data traffic, driven by widespread 5G adoption, immersive AR/VR applications, cloud gaming, and the increasing integration of artificial intelligence (AI), has created an urgent demand for additional spectrum resources in mobile systems [1], [2]. To address this, the International Telecommunication Union (ITU) at the World Radiocommunication Conference (WRC-23) agreed to study the upper mid-band frequency (7–24 GHz), also known as frequency range 3 (FR3), for potential International Mobile Telecommunications (IMT) [3], [4]. However, most of the FR3 frequencies are already occupied by incumbent satellite and fixed-service systems, leading to inevitable spectrum overlap between emerging terrestrial 5G/6G deployments and existing non-terrestrial network (NTN) operations [5], [6]. This overlap raises critical concerns about mutual interference, particularly the interference from dense TN deployments toward the more interference-sensitive NTN downlink receivers [7]. A proper interference characterization and management strategy within the FR3 band is, therefore, crucial to ensure NTN link protection while maintaining terrestrial network (TN) performance.

Recent studies by the satellite and mobile communication industries [5]–[7] have investigated the feasibility of TN–NTN coexistence within the FR3 band. Reports in [5], [6] suggest

that coexistence is generally feasible and predicted a minimal interference impact (<1% outage) on low earth orbit (LEO) satellite user terminals. Reports in [7], however, predict severe non-geostationary satellite orbit (NGSO) interference with outage probabilities exceeding 70% in certain scenarios, underscoring the vulnerability of satellite receivers under dense TN deployments. These contrasting findings motivate further investigation into adaptive interference mitigation within the FR3 band. Existing works have therefore primarily focused on spatial suppression techniques such as interference-nulling beamforming [8], advanced precoder design [9], and dynamic exclusion-zone strategies [3], [4], [10]. In [8], an interference-nulling beamforming approach is proposed for the 12 GHz band, where TN base stations (BSs) steer spatial nulls toward the satellite link to suppress TN-to-NTN interference. Similarly, [9] introduces a hybrid true-time-delay planar-array precoder for three-dimensional null steering. While these methods can effectively reduce cross-system interference, they require precise channel state information (CSI) between the TN and satellite, which is difficult to obtain in practice and highly sensitive to beam misalignment. On the other hand, dynamic exclusion-zone approaches [3], [4], [10] mitigate interference by muting TN base stations near NTN receivers based on satellite trajectory, but this often results in unnecessary coverage gaps and reduced terrestrial throughput.

These limitations highlight the need for more practical and adaptive coexistence strategies. Antenna downtilt control offers an efficient way to reshape the TN radiation pattern and suppress upward interference without relying on complex CSI or precise beam nulling [11]. With the recent introduction of direct satellite-to-cell services, LEO satellites now serve mobile user terminals directly [12]. While protecting fixed satellite gateways is relatively straightforward, mobile NTN users are more vulnerable to interference from TN base stations due to their mobility and variable exposure to sidelobe emissions. Under such dynamic conditions, traditional beamforming and precoding techniques, designed for static NTN receivers, become insufficient. Hence, a joint optimization of TN antenna downtilt and transmit power is required to adaptively mitigate interference toward NTN users. Motivated by these challenges, in this work we develop a unified interference management framework for TN–NTN coexistence in the FR3 band. The contributions of this paper are summarized below.

- We formulate an optimization framework that jointly captures the coupling between TN transmit power, antenna downtilt, and NTN interference constraints. This formulation explicitly models coexistence dynamics, where dense TN deployments must adapt their configurations to protect primary NTN downlink performance.
- To address the non-convex and highly coupled nature of the formulated problem, we develop a Proximal Policy Optimization (PPO)-based reinforcement learning (RL) solution that dynamically learns optimal TN control policies. The proposed method adaptively tunes TN transmit power and antenna downtilt to mitigate NTN interference.
- The simulation results validate the effectiveness of the proposed framework for both static and mobile NTN users. The results demonstrate interference suppression up to 6-8 dB compared to conventional fixed-parameter and exclusion-zone strategies while maintaining over 87% TN gNB availability without extensive muting.

II. SYSTEM MODEL

We consider a spectrum-coexistence scenario in the FR3 upper-mid band, where a TN and an NTN operate in the same geographical region and share the same frequency resources. The TN consists of set of $\mathcal{N} = \{1, 2, \dots, N\}$ 5G gNodeBs (gNBs) serving a set of $\mathcal{U}_{TN} = \{1, 2, \dots, U_{TN}\}$ terrestrial users, while the NTN consists of a single LEO satellite serving a set of $\mathcal{U}_{NTN} = \{1, 2, \dots, U_{NTN}\}$ satellite user terminals. A total system bandwidth B is shared across the region. The geographical area under study lies fully within the instantaneous LEO satellite footprint.

The primary objective of this work is to characterize and mitigate the interference generated by the TN downlink and uplink transmissions toward NTN downlink receivers. In the following subsections, we present the TN and NTN system parameters in depth, followed by the interference-to-noise ratio (INR) characterization.

A. NTN modelling

In the NTN model, the link budget is primarily determined by the propagation geometry and the satellite antenna radiation characteristics.

1) *NTN pathloss*: The NTN links are modeled according to 3GPP TR 38.811 [13]. The *slant distance* between the satellite and the NTN user d at elevation angle α is given by

$$d = \sqrt{R_E^2 \sin^2 \alpha + h_0^2 + 2h_0 R_E - R_E \sin \alpha}, \quad (1)$$

where h_0 is the satellite altitude and R_E is Earth's radius. For a given $d(\alpha)$ and carrier frequency f_c , the free space path loss (FSPL) is expressed as [13],

$$PL_{FS}[dB] = 32.45 + 20 \log_{10}(d) + 20 \log_{10}(f_c), \quad (2)$$

Beyond FSPL, the NTN link suffers from clutter loss (L_{CL}), atmospheric losses, and shadow fading (L_{SF}), both of which depend on whether the link is LOS or Non-Line-of-Sight (NLOS). Thus, the total NTN path loss (PL_{NTN}) is expressed as $PL_{NTN} = PL_{FS} + L_{CL} + L_{SF} + L_{Atm} + L_{IS} + L_{TS}$,

where L_{Atm} is the atmospheric loss, L_{IS} is the ionospheric scintillation loss, and L_{TS} is the tropospheric scintillation loss, and the values are considered as specified in [13].

2) *NTN antenna model*: The LEO satellite is positioned at an altitude of 600 km above Earth's surface and provides communication service to a fixed footprint region of $20 \times 20 \text{ km}^2$ through an always-on spot beam. We adopt the antenna model defined in 3GPP TR 38.811 [13], and its gain pattern is expressed as

$$G_{NTN} = \begin{cases} G_{NTN}^{\max}, & \text{for } \theta = 0, \\ 4 G_{NTN}^{\max} \left| \frac{J_1(ka \sin \theta)}{ka \sin \theta} \right|^2, & \text{for } 0 < |\theta| \leq 90^\circ \end{cases} \quad (3)$$

where G_{NTN}^{\max} dBi is the peak antenna gain, $J_1(\cdot)$ is the Bessel function of the first kind, a is the radius of the antenna's circular aperture, $k = 2\pi f_c/c$ is the wave number, and θ is the angle measured from the bore sight of the antenna's main beam.

B. TN modelling

Following the NTN link characterization, we now define the TN channel and antenna parameters. These parameters directly influence the interference power received by NTN terminals, as discussed later in the INR analysis.

1) *TN pathloss*: The large-scale propagation loss of TN link is modeled using the Urban Macro (UMa) pathloss model, as specified in 3GPP TR 38.901 [14]. The UMa model captures both LOS and NLOS propagation conditions. For the LOS case, the model defines two distance-dependent expressions based on whether the horizontal 2D distance d_{2D} is smaller or larger than the breakpoint distance d'_{th} . The corresponding LOS path loss is given by

$$PL_{LOS}^{UMa} = \begin{cases} 32.4 + 20 \log_{10}(d_{3D}) + 20 \log_{10}(f_c), & 10 \text{ m} \leq d_{2D} < d'_{th}, \\ 32.4 + 40 \log_{10}(d_{3D}) + 20 \log_{10}(f_c) - 10 \log_{10}(d'^2_{th} + (h_{BS} - h_{UT})^2), & d'_{th} \leq d_{2D} \leq 5 \text{ km}. \end{cases} \quad (4)$$

where d_{3D} is the 3-D distance. h_{BS} and h_{UT} represent the height of the gNB and the TN user terminal, respectively.

2) *TN antenna modelling*: We model the radiation characteristics of TN gNB antennas in accordance with 3GPP TR 38.901 [14]. Each gNB antenna pattern is defined by three parameters: the horizontal angle relative to the antenna boresight ϕ' , the vertical angle θ' , and the downtilt angle θ_d . For a given ϕ' and θ' , the antenna gain of TN gNB is

$$G_{BS}(\theta', \phi') = G_{\max} - \min\{-[G_V(\theta') + G_H(\phi')], A_{\max}\}. \quad (5)$$

where G_{\max} is the maximum directional gain, and A_{\max} is the maximum front-to-back attenuation limit. The horizontal and vertical gain are given by $G_H(\phi') = -\min\left[12\left(\frac{\phi'}{\phi'_{3dB}}\right)^2, A_{\max}\right]$, and $G_V(\theta') = -\min\left[12\left(\frac{\theta' - \theta_d}{\theta'_{3dB}}\right)^2, SLA_V\right]$, respectively,

with $\phi'_{3\text{dB}}$ and $\theta'_{3\text{dB}}$ being the horizontal and vertical half-power bandwidth (HPBW). SLA_V represents the side-lobe attenuation.

C. Interference-to-Noise Ratio (INR)

Based on the established TN and NTN link models, we now analyze the mutual interference characteristics arising from their coexistence in the same frequency band. Since both systems share the FR3 spectrum, TN transmissions can introduce significant interference to the NTN downlink, which is particularly sensitive due to the long propagation path and limited link margin [1]. To quantify this effect, we consider the interference-to-noise ratio (INR) as a key performance indicator representing the ratio of aggregated interference power to the receiver noise floor. For each considered gNB location and antenna configuration, we compute the interference at each NTN user terminal.

1) *Interference due to downlink TN*: The interference received at NTN user terminal $n \in \mathcal{U}_{NTN}$ from the $i \in \mathcal{N}$ TN gNB is

$$I_{n,i}^{DL} = P_i^{gNB} + G_{BS}(\theta', \phi') + G_{NTN}^{UT}((\theta'_{n,i})) - PL(d_{n,i}), \quad (6)$$

where P_i^{gNB} is the transmitting power of i^{th} gNB, G_{NTN}^{UT} is the NTN user antenna gain, $\theta'_{n,i}$ is the angle between the n^{th} NTN user terminal's boresight and i^{th} gNB's interference axis, $PL(\cdot)$ is the pathloss, and $d_{n,i}$ is the distance between n^{th} NTN user terminal and i^{th} gNB.

2) *Interference due to uplink TN*: Similarly, the interference received at NTN user terminal $n \in \mathcal{U}_{NTN}$ from TN user $i \in \mathcal{U}_{TN}$ is given by, $I_{n,i}^{UL} = P_i^{UE} + G_{UE}(\theta', \phi') + G_{NTN}^{UT}((\theta''_{n,i})) - PL(d'_{n,i})$, where P_i^{UE} is the TN user uplink power, G_{UE} is the user antenna gain, $\theta''_{n,i}$ is the angular offset between the TN UE and NTN terminal, and $d'_{n,i}$ is the distance between TN and NTN user terminal.

3) *Aggregated INR*: Considering the effect of interference from both downlink and uplink TN transmission, the aggregated INR (in dB) at the NTN user $n \in \mathcal{U}_{NTN}$ is expressed as

$$INR_n = 10 \log_{10} \left(\sum_{i \in \mathcal{N}} I_{n,i}^{DL} \right) + 10 \log_{10} \left(\sum_{i \in \mathcal{U}_{NTN}} I_{n,i}^{UL} \right) - 10 \log_{10}(kTB) \quad (7)$$

where k represents the Boltzmann constant, T is the temperature, and B is the NTN user terminal bandwidth. Typically, INR quantifies the interference penalty experienced by an NTN user terminal [4]. An NTN terminal is considered interfered with when its INR exceeds a specified protection threshold. Typically, the protection threshold range spanning from -12.2 dB to -6 dB [7], [10].

D. NTN aggregated downlink throughput

The quantified INR directly impacts the achievable NTN downlink rate. The aggregated downlink throughput of the NTN system is determined by Shannon's capacity equation as follows,

$$\mathcal{R}_{NTN} = B \sum_{n \in \mathcal{U}_{NTN}} \log_2(1 + \gamma_n), \quad (8)$$

where B represents the total NTN bandwidth. γ_n represents the corresponding signal-to-interference-and-noise-ratio (SINR) of NTN user $n \in \mathcal{U}_{NTN}$, defined as

$$\gamma_n = \frac{P_n^{rx}}{\sum_{i \in \mathcal{N}} I_{n,i} + \sum_{i \in \mathcal{U}_{NTN}} I_{n,i}^{UL} + N_0}, \quad (9)$$

where P_n^{rx} is the received power at NTN user terminal and N_0 is the noise power spectral density.

The NTN downlink throughput depends on both TN transmit power and antenna configurations, which jointly determine the interference experienced by NTN users. We next formulate an optimization problem to identify optimal TN control parameters that preserve NTN performance while satisfying FR3 coexistence constraints.

III. PROBLEM FORMULATION

Building on the INR and throughput relationships, in this section, we formalize the optimization problem for TN-NTN coexistence. Interference from TN downlink transmissions poses a critical challenge to maintaining reliable NTN downlink performance. On the downlink side, adaptive transmit power control at TN gNBs can directly control the radiated energy toward the satellite footprint, while antenna downtilt adjustment provides an additional degree of freedom to reshape the vertical radiation pattern and suppress undesired emissions toward NTN users. Consequently, a coordinated control strategy that jointly optimizes gNB transmit power and antenna downtilt is essential to balance NTN protection and TN performance. The optimization problem is formulated as

$$\max_{\mathbf{P}^{gNB}, \boldsymbol{\theta}_d} \mathcal{R}_{NTN}(\mathbf{P}^{gNB}, \boldsymbol{\theta}_d) \quad (10)$$

$$\text{s.t. } INR_n(\mathbf{P}^{gNB}, \boldsymbol{\theta}_d) \leq \Gamma_{\text{th}}, \quad \forall n, \quad (11)$$

$$\theta_{d,i}^{\min} \leq \theta_{d,i} \leq \theta_{d,i}^{\max}, \quad \forall i \in \mathcal{N}, \quad (12)$$

$$P_i^{gNB} \leq P_{\max}, \quad \forall i \in \mathcal{N}, \quad (13)$$

where $\mathbf{P}^{gNB} = [P_1^{gNB}, \dots, P_N^{gNB}]$ represents the transmit power vector of TN gNBs and $\boldsymbol{\theta}_d = [\theta_{d,1}, \dots, \theta_{d,N}]$ denotes the corresponding antenna downtilt configuration. Constraint (11) ensures that the INR experienced by each NTN user remains below the protection threshold Γ_{th} . The downtilt bound in (12) limits the gNB tilt angle within its feasible mechanical range to control interference without compromising terrestrial coverage. Finally, the downlink power constraint in (13) restricts each gNB's transmit power below P_{\max} .

The formulated optimization problem is inherently difficult to solve due to strong nonlinear coupling among TN transmit power (\mathbf{P}^{gNB}), and antenna downtilt ($\boldsymbol{\theta}_d$). Furthermore, the SINR and INR expressions involve logarithmic and fractional terms, rendering the objective function highly nonconvex and non-differentiable. Conventional convex optimization methods fail to capture these complex dynamics or guarantee convergence to a global solution. To overcome these limitations, we adopt a reinforcement learning (RL)-based approach to iteratively learn adaptive power-tilt control policies under dynamic interference environments.

IV. PROPOSED SOLUTION APPROACH

To this end, we propose a centralized RL-based framework employing the Proximal Policy Optimization (PPO) algorithm. The centralized agent is deployed at the core network level, coordinating the joint adaptation of TN base station transmit power, user uplink power, and antenna downtilt across the shared FR3 spectrum. The overall framework illustrated in Fig. 1, operates through a closed-loop interaction between the TN-NTN systems and the centralized learning process. The TN and NTN entities periodically report network state information, such as interference levels, active gNB status, and NTN throughput, to the core network. The centralized PPO agent processes this information, evaluates interference conditions, and issues optimized control commands to the TN system. In addition to power and antenna downtilt control actions, we introduce a selective sector muting mechanism as a discrete control action. In dense urban deployments, certain BS sectors may continue to generate harmful interference toward NTN users even after power and tilt adjustments. Temporarily muting such sectors during critical NTN downlink periods provides a flexible and localized interference mitigation measure without requiring a full network shutdown.

A. Observation and Action Space

At each decision step t , the PPO agent observes a state vector s_t representing the interference and activity conditions across the TN-NTN coexistence environment, and selects an action vector a_t that jointly controls TN transmission and configuration parameters. The observation space \mathcal{S} is defined as

$$\mathcal{S} = \{s_t = [\theta_{EL,t}, \eta_t, \mathcal{R}_{NTN,t}, \chi_t, \Gamma_{th}]\}, \quad (14)$$

where θ_{EL} denotes the satellite elevation angle, η_t represents the percentage of NTN user terminals experiencing harmful interference (i.e., INR $> \Gamma_t$), $\mathcal{R}_{NTN,t}$ is the aggregated NTN throughput, χ_t is the percentage of active TN gNBs, and Γ_{th} represents the current INR protection threshold in use.

The action space \mathcal{A} defines the control variables that the PPO agent can adjust at each step, and is given by

$$\mathcal{A} = \{a_t = [\Gamma_{th,t}^{new}, \delta_{i,t}, P_{i,t}^{gNB}, P_{i,t}^{UE}, \theta_{d,i,t}]\}, \quad i \in \mathcal{N}, \quad (15)$$

where $\Gamma_{th,t}^{new}$ represents the updated INR protection threshold; $\delta_{i,t} \in \{0, 1\}$ denotes the binary sector muting control; $P_{i,t}^{gNB} \in [P_{min}, P_{max}]$ dBm and $P_{i,t}^{UE} \in [P_{min}^{UE}, P_{max}^{UE}]$ dBm are the downlink and uplink transmit powers of TN gNB and UEs, respectively, and $\theta_{d,i,t} \in [\theta_{d,i}^{min}, \theta_{d,i}^{max}]$ specifies the TN gNB antenna downtilt angle.

B. Reward function

The immediate reward r_t at time step t is designed to guide the PPO agent toward maximizing NTN performance while ensuring TN continuity and limiting harmful interference. It is expressed as a weighted sum of normalized throughput, TN activity, and interference penalty terms, as expressed below

$$r_t = w_1 \bar{\mathcal{R}}_{NTN,t} + w_2 \chi_t - w_3 \eta_t, \quad (16)$$

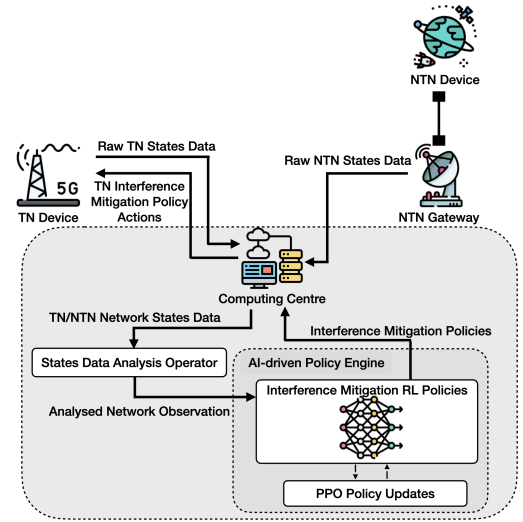


Figure 1. Interference Mitigation RL System

where $\bar{\mathcal{R}}_{NTN,t} = \frac{\mathcal{R}_{NTN,t}}{\mathcal{R}_{NTN,t}^{max}}$ denotes the normalized NTN downlink throughput, and $\chi_t = \frac{N_{Active}}{N}$ denotes the fraction of active TN gNBs. The coefficients w_1 , w_2 , and w_3 control the trade-off between NTN throughput maximization, interference suppression, and TN service continuity.

C. PPO for TN-NTN coexistence

We use the Proximal Policy Optimization (PPO) algorithm as the learning backbone of the proposed centralized framework, balancing stable policy improvement with efficient training. PPO is an actor-critic-based reinforcement learning method that maintains two neural networks [15], [16]. An actor that parameterizes the policy $\pi_\theta(a_t|s_t)$ to select actions, and a critic that estimates the state-value function $V_\phi(s_t)$ to evaluate the long-term quality of those actions. During training, the actor interacts with the TN-NTN environment to collect trajectories of states, actions, and rewards. The advantage function, $A_t = \hat{R}_t - V_\phi(s_t)$, measures how much better an action performed is compared to the expected baseline value, and guides the policy update. To ensure stable learning, PPO maximizes a clipped surrogate objective that constrains large policy updates through a ratio term $r_t(\theta) = \frac{\pi_\theta(a_t|s_t)}{\pi_{\theta_{old}}(a_t|s_t)}$. The objective is given by $L^{PPO}(\theta) = \mathbb{E}_t [\min (r_t(\theta) A_t, \text{clip}(r_t(\theta), 1 - \epsilon, 1 + \epsilon) A_t)]$, where ϵ is a clipping parameter that limits the deviation between new and old policies, preventing performance collapse due to overly aggressive updates. The critic network minimizes the value loss $\mathcal{L}_V = (V_\phi(s_t) - \hat{R}_t)^2$, enabling better estimation of expected returns.

Through alternating actor-critic updates, PPO efficiently learns stable and adaptive control strategies for power adjustment, antenna downtilt tuning, and sector muting. The following section presents the simulation setup and performance evaluation results to validate the effectiveness of the proposed learning-based coexistence framework.

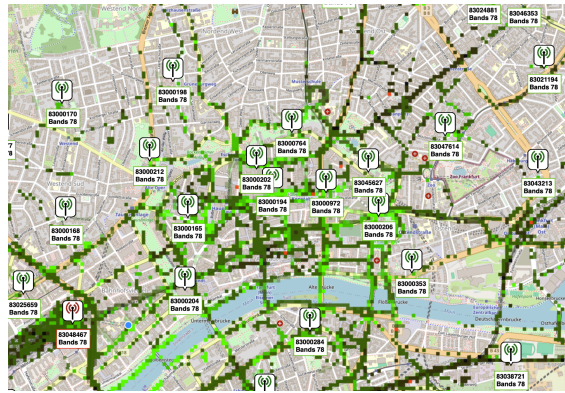


Figure 2. Base Station Map (Frankfurt)

Table I
ENVIRONMENT SETUP PARAMETERS

Parameters	Value
Carrier frequency	12 GHz
Total bandwidth	200 MHz
Number of gNBs in beam footprint	106
UEs per TN gNB Cell	12 – 20
Satellite Tx power	48 dBm
Satellite antenna gain	38.3 dBi
Dish terminal antenna gain	33 dBi
Direct-to-cell device antenna gain	17 dBi
TN gNBs max Tx power	33 dBm
TN UEs max Tx power	23 dBm

V. PERFORMANCE EVALUATION

A. Simulation setup

We consider a TN-NTN coexistence scenario where NTN user terminals are spatially distributed according to a homogeneous Poisson Point Process (PPP) within a $20 \times 20 \text{ km}^2$ LEO satellite spot-beam footprint. Two types of NTN users are considered: fixed gateway terminals (T1) with high-gain, narrow-beam antennas, and direct-satellite-to-cell mobile terminals (T2) with low-gain, wide-beam antennas. Simulations are performed for varying NTN user densities: 6×10^{-8} , 1×10^{-7} , and 3×10^{-7} users/m 2 , corresponding to 24, 40, and 120 active terminals, respectively. Additionally, different T1:T2 user ratios are examined to capture the impact of antenna characteristics and spatial load on TN-to-NTN interference. To capture dynamic link evolution during a satellite pass, one snapshot is recorded for every 1° change in the LEO satellite elevation angle. For a 500 km LEO orbit with 53° inclination, the snapshot interval varies from roughly 1 s near zenith to 10 s near the horizon. The full visible pass is defined over the 10° to 170° elevation, yielding 160 simulation snapshots.

The terrestrial network layout is constructed from real base station data for Frankfurt am Main, mapped within the same $20 \times 20 \text{ km}^2$ region, as shown in Fig. 2. Each BS retains its real-world coordinates, while TN user terminals are generated following a homogeneous PPP with density $1.3 \times 10^{-5} \text{ users/m}^2$ and associated with the nearest BS. All the key simulation parameters are summarized in Table I.

Baseline methodologies: To benchmark the effectiveness of the proposed PPO-based framework, we compare its performance against two baseline interference-management schemes. The first is a *no-coordination* scenario, where the TN operates without any NTN-aware coordination or interference control, and the gNBs transmit with fixed power and antenna settings. The second is the rule-based *ASCENT approach* [10], which employs deterministic exclusion zones and threshold-based mute/unmute rules to protect NTN receivers, typically improving NTN protection at the expense of TN coverage.

B. Results and discussion

PPO Training Convergence: Figure 3 illustrates the PPO training convergence across random seeds. Blue traces represent

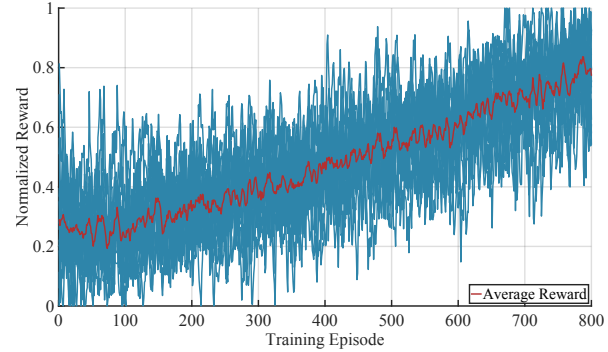


Figure 3. PPO Training Convergence across Random Seeds

the normalized episodic rewards, while the red curve denotes their running average. The steadily increasing average reward indicates stable learning and consistent policy improvement, despite inherent variability in individual episodes typical of stochastic interference-management environments.

Effect of NTN user density: Figure 4 compares INR cumulative distribution functions for low (6×10^{-8}), medium (1×10^{-7}), and high (3×10^{-7}) NTN user densities under different interference-management schemes. Here, only T1 fixed gateway NTN users are considered. Across all densities, the proposed PPO-based method provides robust interference suppression compared to both ASCENT and the no-coordination baseline. While ASCENT achieves its best performance under high-density conditions, where its threshold-based muting is frequently triggered, but its static exclusion rules become overly conservative and inefficient at lower densities. In contrast, the proposed learning-based framework adapts its actions to the INR threshold, leveraging selective sector muting, transmit-power control, and antenna downtilt adjustments. This enables efficient interference mitigation without resorting to large-scale TN shutdowns, thereby maintaining stable NTN protection across all densities.

Effect of NTN User Types: Figure 5 compares INR distributions for varying T1:T2 NTN user ratios, where 100 : 0 (all fixed gateways), 50 : 50 (mixed), and 0 : 100 (all direct-to-cell devices). Scenarios dominated by T1 users yield lower INR due to their high-gain, narrow-beam antennas, while higher propor-

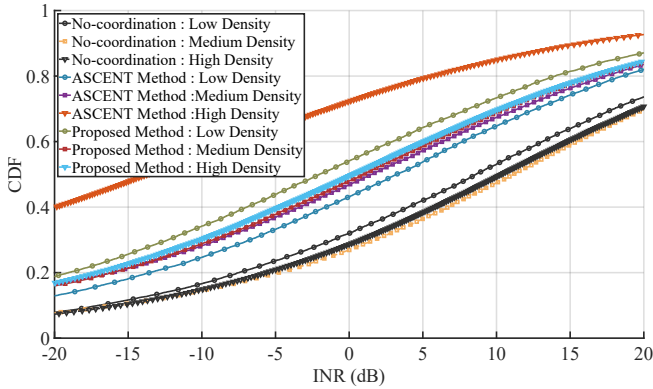


Figure 4. INR Comparison across NTN Densities

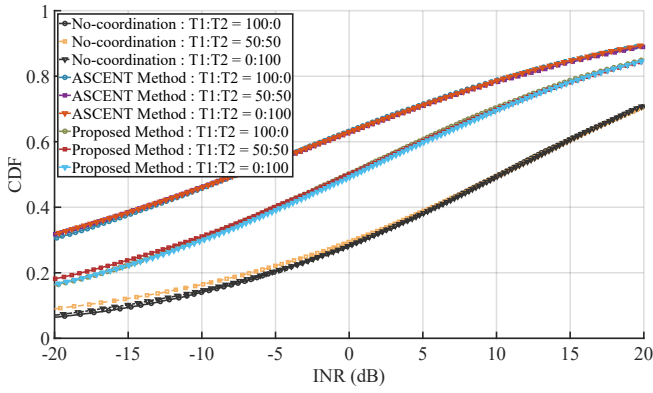


Figure 5. INR Comparison across NTN User Types

tions of T2 users result in greater interference exposure. Across all user mixes, the proposed PPO-based approach achieves median INR improvements of 6–8 dB over ASCENT and the no-coordination baseline. The proposed framework effectively suppresses TN interference for both user types, with clear gains for direct-to-cell users.

Effect on TN Base-Station Activeness: Figure 6 illustrates the active BS ratio across NTN densities, reflecting how each scheme balances NTN protection with TN service continuity. ASCENT shows a steep decline in activeness, from 79.43% at low density to 28.37% at high density, indicating that its lower INR (as shown in Figure 4) comes primarily from extensive muting rather than efficient interference management. In contrast, the proposed RL framework sustains a consistently high activeness level ($\sim 87\%$) across densities, supported by its adaptive per-sector control. This demonstrates that the proposed approach not only achieves the interference suppression trends observed in Fig. 4 and Fig. 5 but does so while preserving TN operational availability and avoiding unnecessary muting.

VI. CONCLUSION

In this work, we developed an RL-based interference management framework to enable practical TN–NTN coexistence in the FR3 band. By jointly optimizing TN downlink power, antenna downtilt, and selective muting through a centralized PPO agent, the proposed approach dynamically adapts to vary-

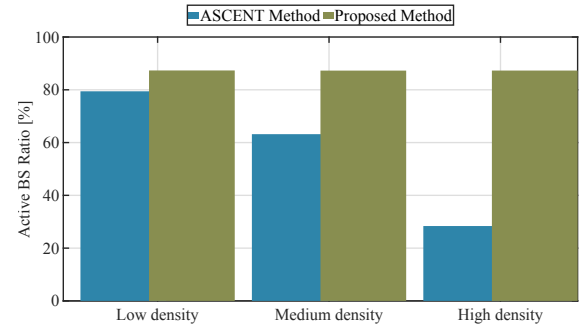


Figure 6. TN Base Station Activeness Comparison

ing interference and network conditions. Simulation results confirmed that the PPO-based control policy substantially enhances NTN downlink throughput and interference protection while maintaining TN activity in the overlap region, outperforming static power control and exclusion-zone methods.

ACKNOWLEDGMENT

This work was partially funded by the Federal Ministry of Education and Research Germany within the project “Open6GHub” under grant 16KISK012.

REFERENCES

- [1] P. Testolina, M. Polese, and T. Melodia, “Sharing Spectrum and Services in the 7–24 GHz Upper Midband,” *IEEE Commun. Mag.*, vol. 62, no. 8, pp. 170–177, 2024.
- [2] M. Na *et al.*, “Operator’s Perspective on 6G: 6G Services, Vision, and Spectrum,” *IEEE Commun. Mag.*, vol. 62, no. 8, pp. 178–184, 2024.
- [3] Z. Hassan *et al.*, “Spectrum Sharing of the 12 GHz Band with Two-Way Terrestrial 5G Mobile Services: Motivations, Challenges, and Research Road Map,” *IEEE Commun. Mag.*, vol. 61, no. 7, pp. 53–59, 2023.
- [4] T.-S. R. Niloy *et al.*, “Interference Analysis of Coexisting 5G Networks and NGSO FSS Receivers in the 12-GHz Band,” *IEEE Wireless Communications Letters*, vol. 12, no. 9, pp. 1528–1532, 2023.
- [5] RKF Engineering Solutions, LLC, “Assessment of feasibility of coexistence between NGSO FSS Earth Stations and 5G operations in the 12.2 – 12.7 GHz band,” Tech. Rep., 2021.
- [6] RSAcces, “Two New Studies Show a Win-Win in 12 GHz Band for Consumers and American 5G Leadership,” RSAcces, Tech. Rep., 2021.
- [7] Space Exploration Corp., “SpaceX analysis of the effect of terrestrial mobile deployment on ngso fss downlink operations,” Tech. Rep., 2022.
- [8] S. Kang *et al.*, “Terrestrial-Satellite Spectrum Sharing in Upper Mid-Band with Interference Nulling,” in *Proc. IEEE ICC*, 2024, pp. 5057–5062.
- [9] A. Wadaskar and D. Cabric, “Satellite-Terrestrial Coexistence in FR3 Band via Hybrid True-Time-Delay Array-based Nulling,” in *Proc. IEEE DySPAN*, 2025, pp. 1–10.
- [10] T.-S. R. Niloy *et al.*, “ASCENT: A Context-Aware Spectrum Coexistence Design and Implementation Toolset for Policymakers in Satellite Bands,” in *Proc. IEEE DySPAN*, 2024, pp. 240–248.
- [11] E. Tekgul *et al.*, “Joint Uplink-Downlink Capacity and Coverage Optimization via Site-Specific Learning of Antenna Settings,” *IEEE Transactions on Wireless Communications*, vol. 23, no. 5, pp. 4032–4048, 2024.
- [12] D. Tuzi *et al.*, “Distributed Approach to Satellite Direct-to-Cell Connectivity in 6G Non-Terrestrial Networks,” *IEEE Wireless Communications*, vol. 30, no. 6, pp. 28–34, 2023.
- [13] 3GPP TR 38.811, “Study on New Radio to support non-terrestrial networks,” Jun. 2019.
- [14] 3GPP TR 38.901, “Study on channel model for frequencies from 0.5 to 100 GHz,” Mar. 2021.
- [15] N. Keshtiarast, O. Renaldi, and M. Petrova, “Wireless MAC Protocol Synthesis and Optimization With Multi-Agent Distributed Reinforcement Learning,” *IEEE Networking Letters*, vol. 6, no. 4, pp. 242–246, 2024.
- [16] J. Schulman, F. Wolski, P. Dhariwal, A. Radford, and O. Klimov, “Proximal policy optimization algorithms,” 2017. [Online]. Available: <https://arxiv.org/abs/1707.06347>